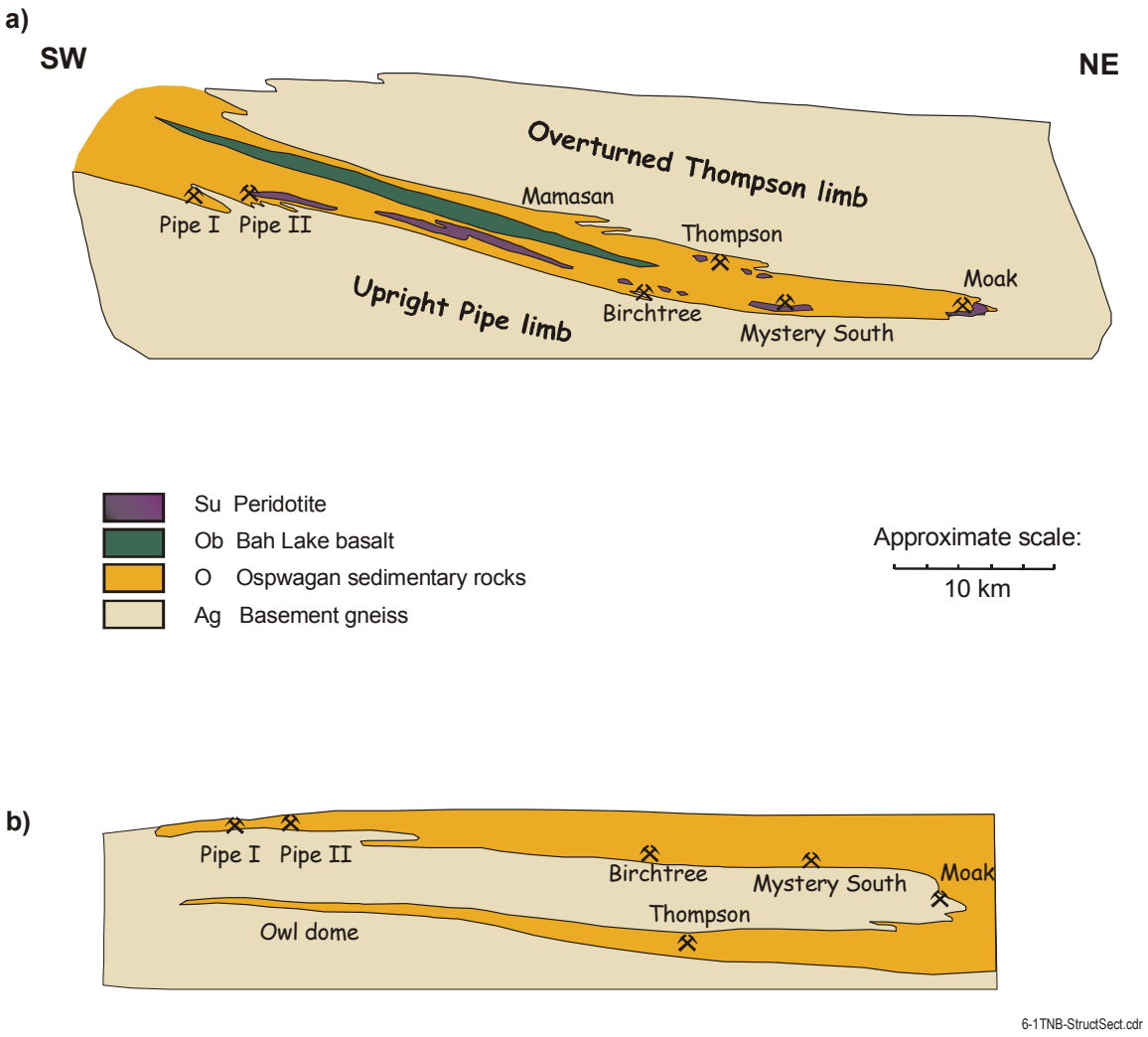

Figure 6.1 Schematic longitudinal sections through proposed fold nappes. The sections are oriented parallel to the main upright folds, which are therefore ignored. See **Figure 6.2** for interpretation. a) Section from Bleeker, 1990a, showing a single synclinal nappe, and location of mines in the structure. b) Section from Golightly and Lyons, 1996, showing an alternate interpretation involving two synclinal nappes with different vergence than in (a).

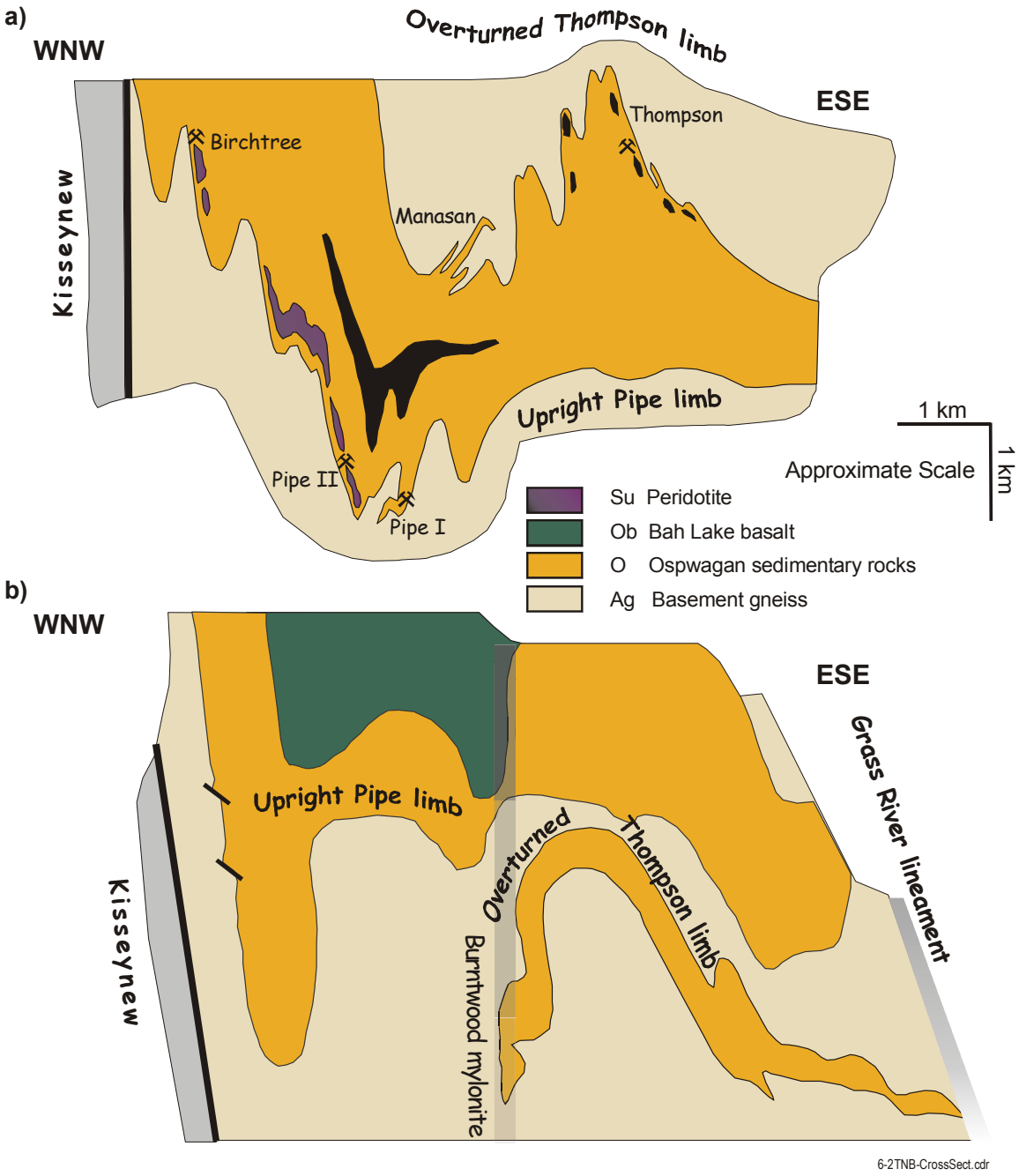

Figure 6.2 Schematic cross-sections through the regional structures, showing possible relationships in the northern and central TNB projected onto a composite profile.

a) Interpretation as a single synclinal nappe of the Ospwagan Group above upright basement gneiss and below an inverted basement cap, taken from Bleeker (1990a). This interpretation is consistent with the southwest vergence suggested by new structural mapping at Setting Lake (cross-section in prep.) A revised structural history suggests that overturning occurred progressively during D_2 and D_3.

b) Interpretation as two large, refolded recumbent synclines projected toward the 'Owl dome', after Golightly and Lyons (1996). In this section, the upright 'Pipe limb' projects above the Thompson structure, separated by an anticlinal basement nappe with a westerly dipping enveloping surface. At Thompson, such folds require juxtaposition along the Burntwood mylonite zone.

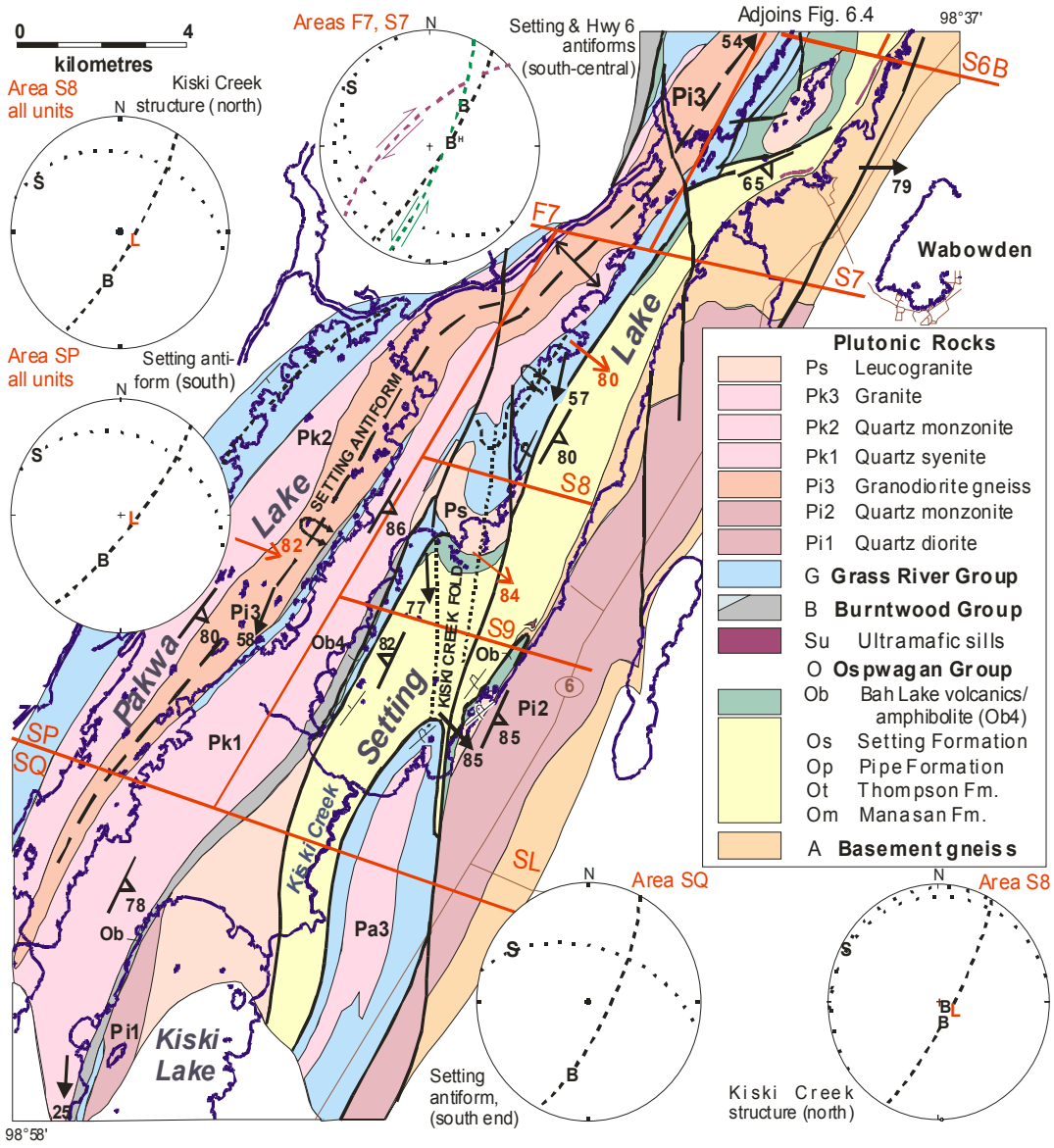

Figure 6.3 Simplified geological map, structural interpretation, and equal-area stereograms of southern Setting Lake. Structural subareas are outlined and labelled in the same fashion as the corresponding synoptic stereograms. The full data are given in **Figures 6.5** to **6.9**. Mean foliation planes, mean lineations and mean fold axes plotted on the map are taken from the stereoplots. Structural and stereographic symbols are given in **Figure 6.4**. Major structures are discussed in the text.

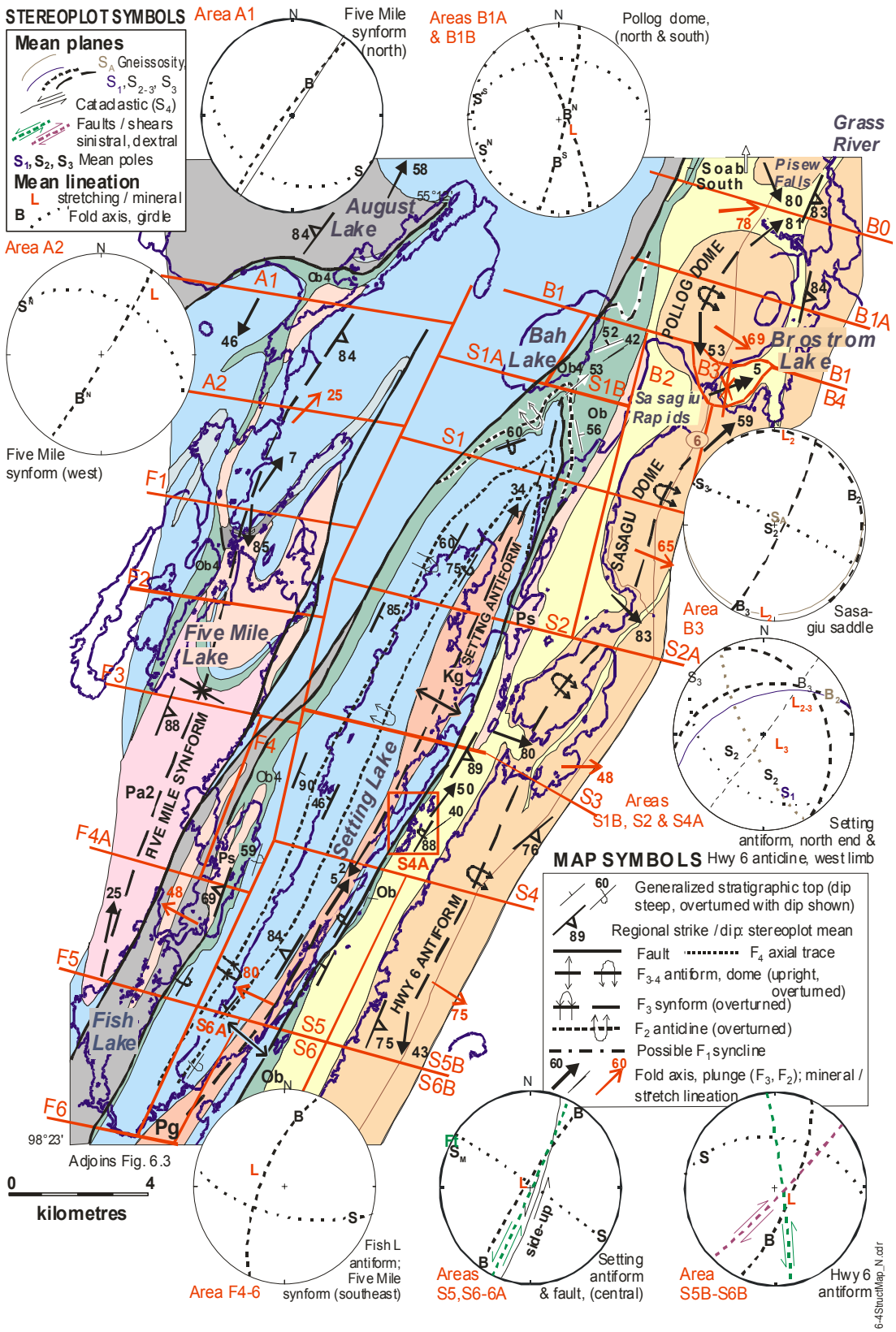

Figure 6.4 Simplified map, structural interpretation, and stereograms of northern Setting Lake. (See caption of **Figure 6.3** for more details).

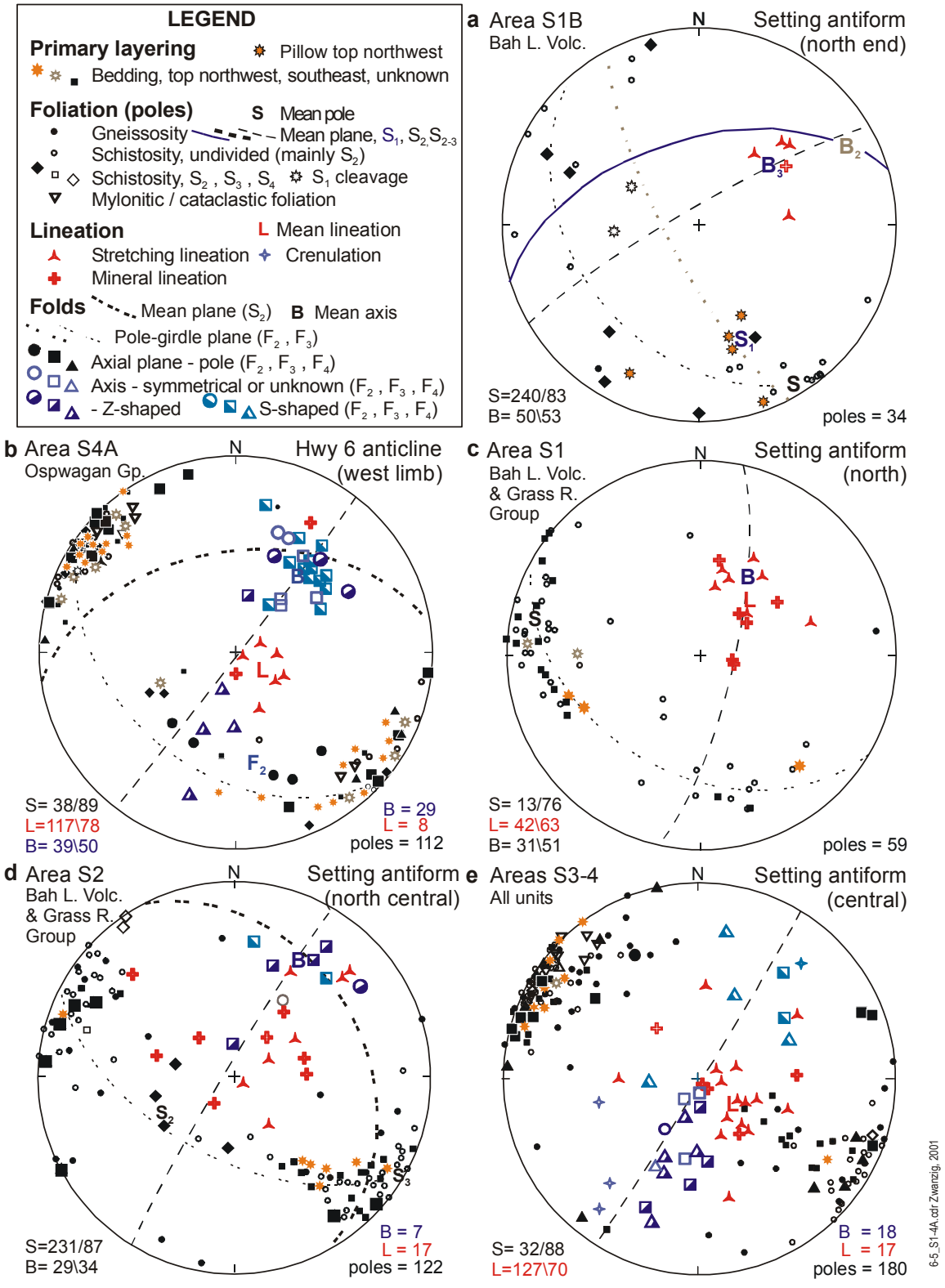

Figure 6.5 Equal-area stereograms of the fabric elements in the northern Setting Lake area, organized into the structural sub-areas shown on **Figure 6.4**.

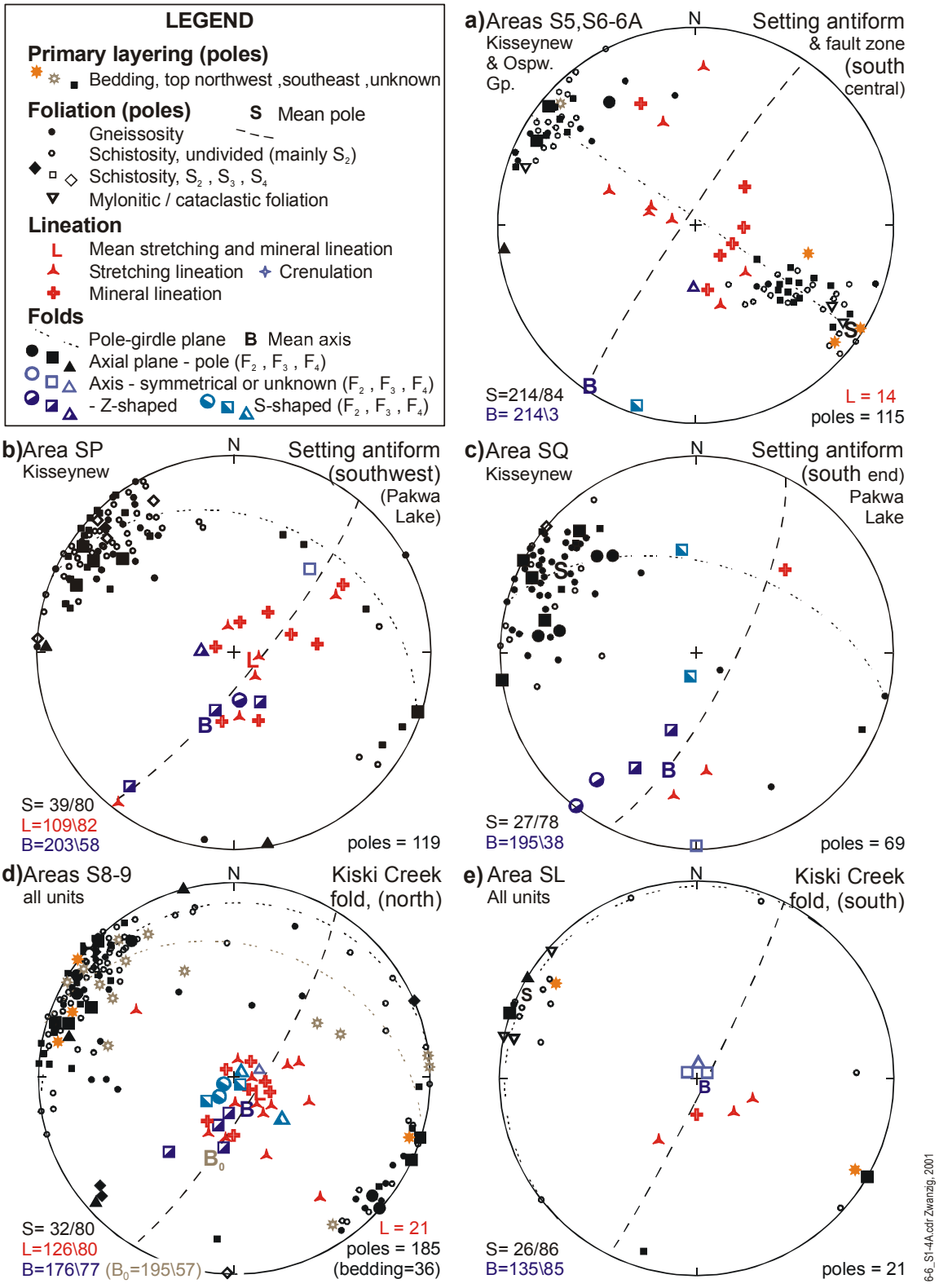

Figure 6.6 Equal area stereograms of the fabric elements in the southern Setting and Pakwa Lake areas, organized into the structural sub-areas shown on **Figures 6.3** and **6.4**.

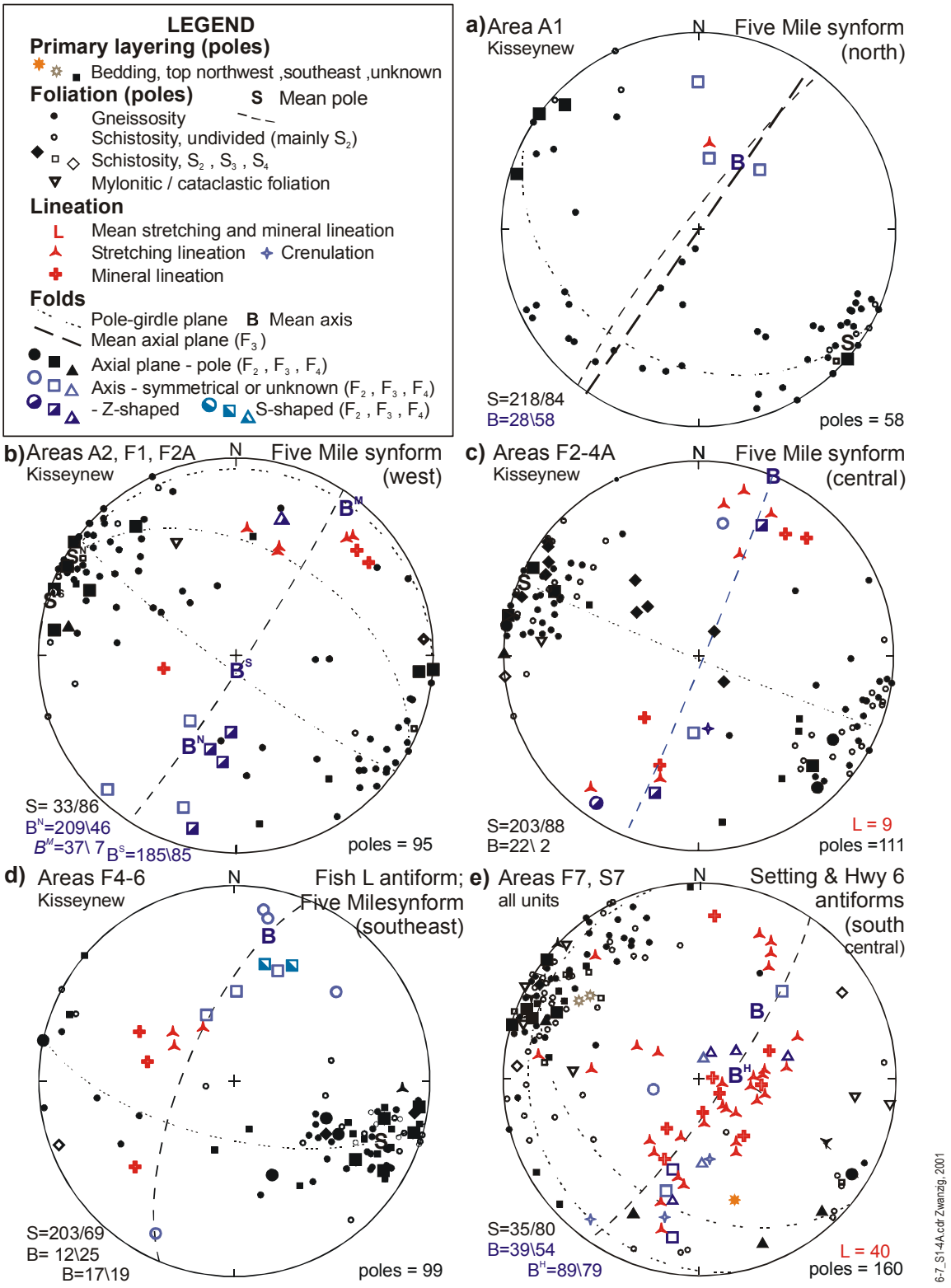

Figure 6.7 Equal-area stereograms of the fabric elements west of the Setting Lake area, organized into the structural sub-areas shown on **Figures 6.3** and **6.4**.

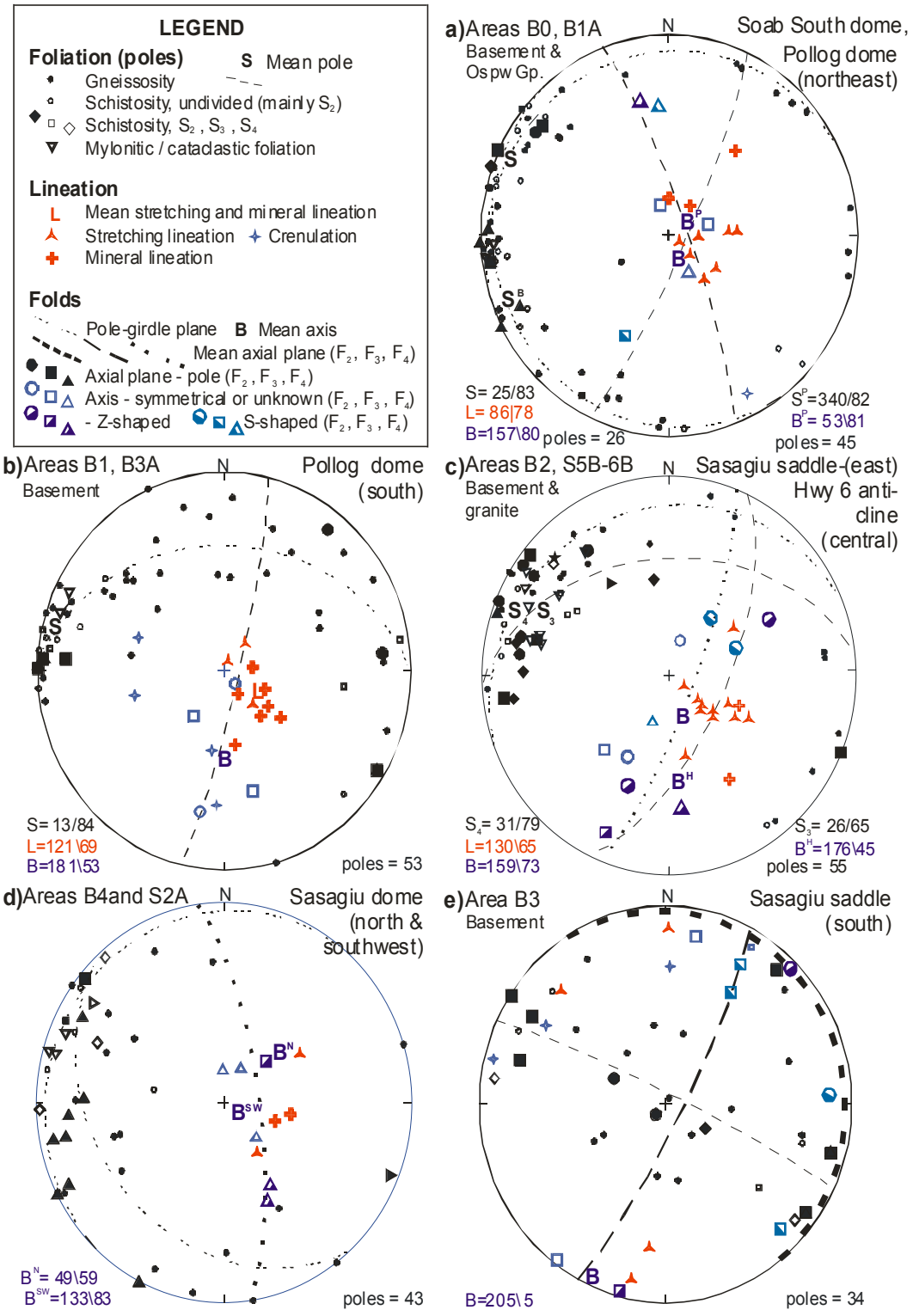

Figure 6.8 Equal-area stereograms of the fabric elements north of the Setting Lake area, organized into the structural sub-areas shown on **Figure 6.4**.

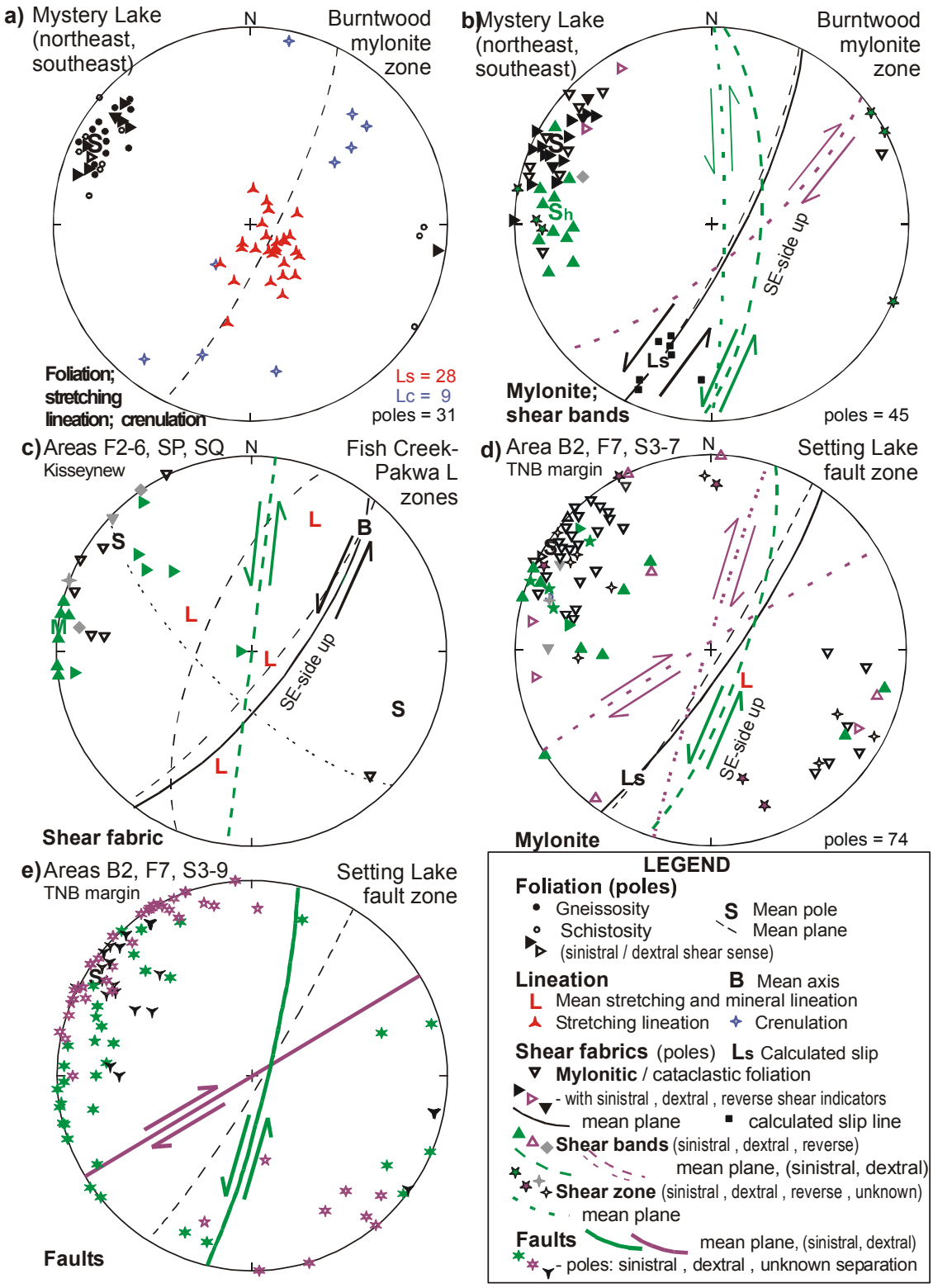

Figure 6.9 Equal-area stereograms of fabric elements and structures related to mylonite, shear zones and faults, associated with the high-strain zones shown on **Figures 6.3** and **6.4**.

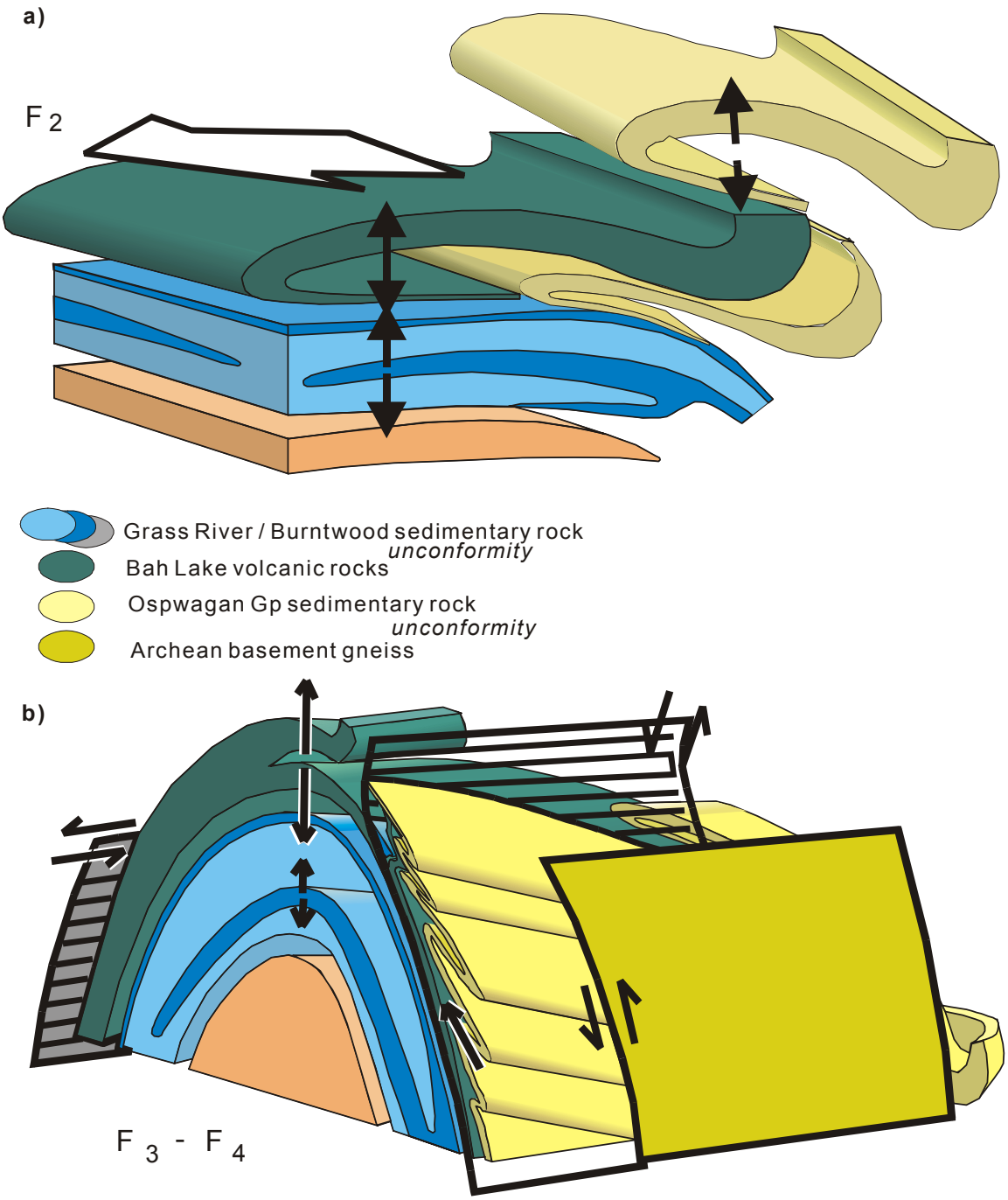

Figure 6.10 a) Southwest-verging F_2 major folds have produced overturning of the Ospwagan Group onto Kisseynew sedimentary rocks (Grass River Group), also tightly folded during F_2. The folds are interpreted to have been originally recumbent, and to have formed during the local metamorphic peak and regional foliation development (S_2). b) The F_2 structures were refolded by an F_3-F_4 upright antiform. Large F_3 folds in the Setting Formation (S_2), parasitic to the major antiform, are upward facing. They indicate that the Ospwagan Group was overturned during a late phase (F_3). The basement unconformity is highly sheared; the contacts between Bah Lake volcanic rocks and Grass River and Burntwood sedimentary rocks are prominent faults.

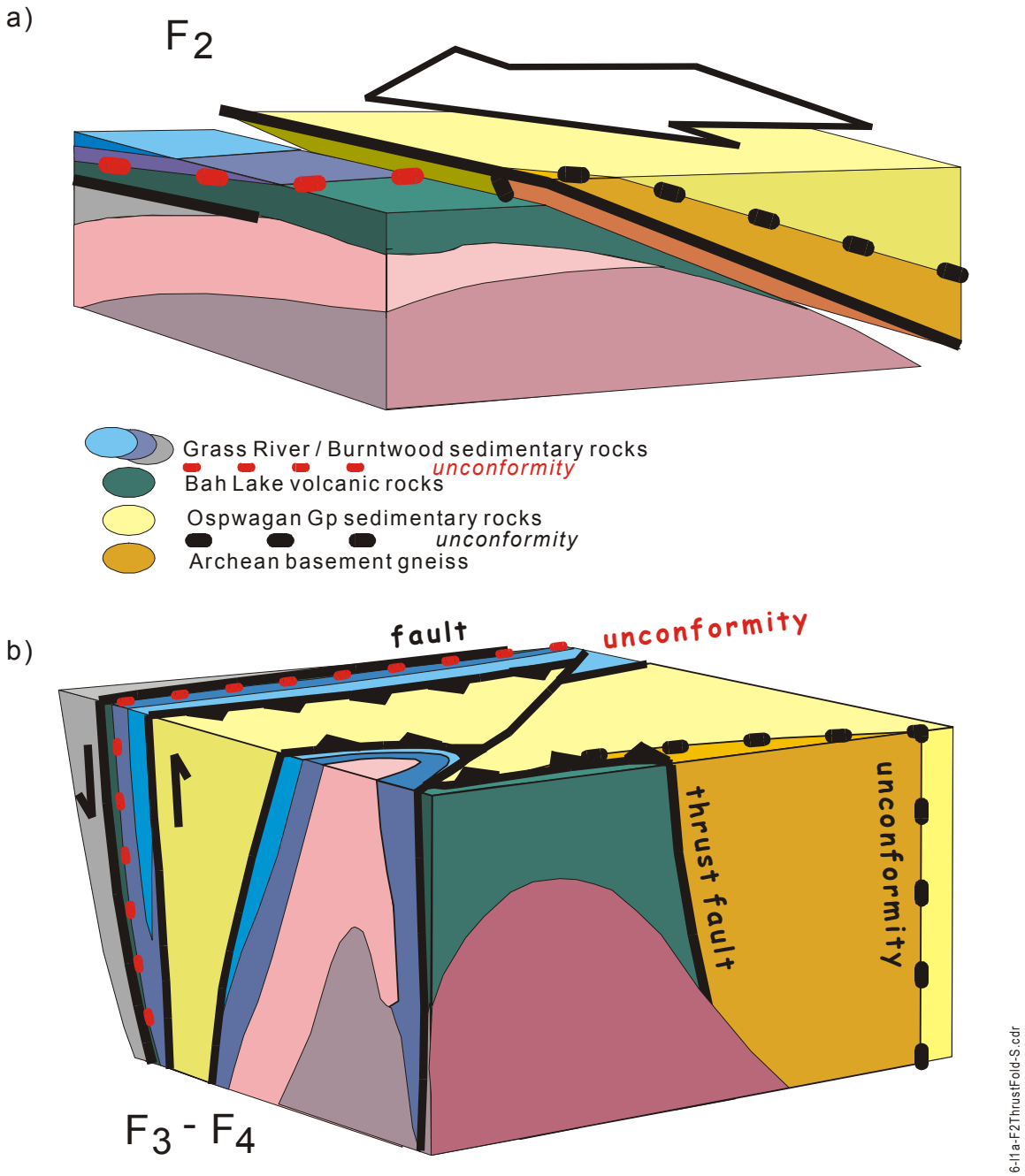

Figure 6.11 a) Interpretation of structural relationships at the south end of Setting Lake suggest that a full section of Ospwagan Group resting unconformably on a sliver of basement gneiss was thrust over the Bah Lake assemblage, and farther south over the Grass River Group. b) Tight F_3- F_4 folds and late faults have deformed the early thrust and produced a subvertical plunge in the Kiski Creek structure.

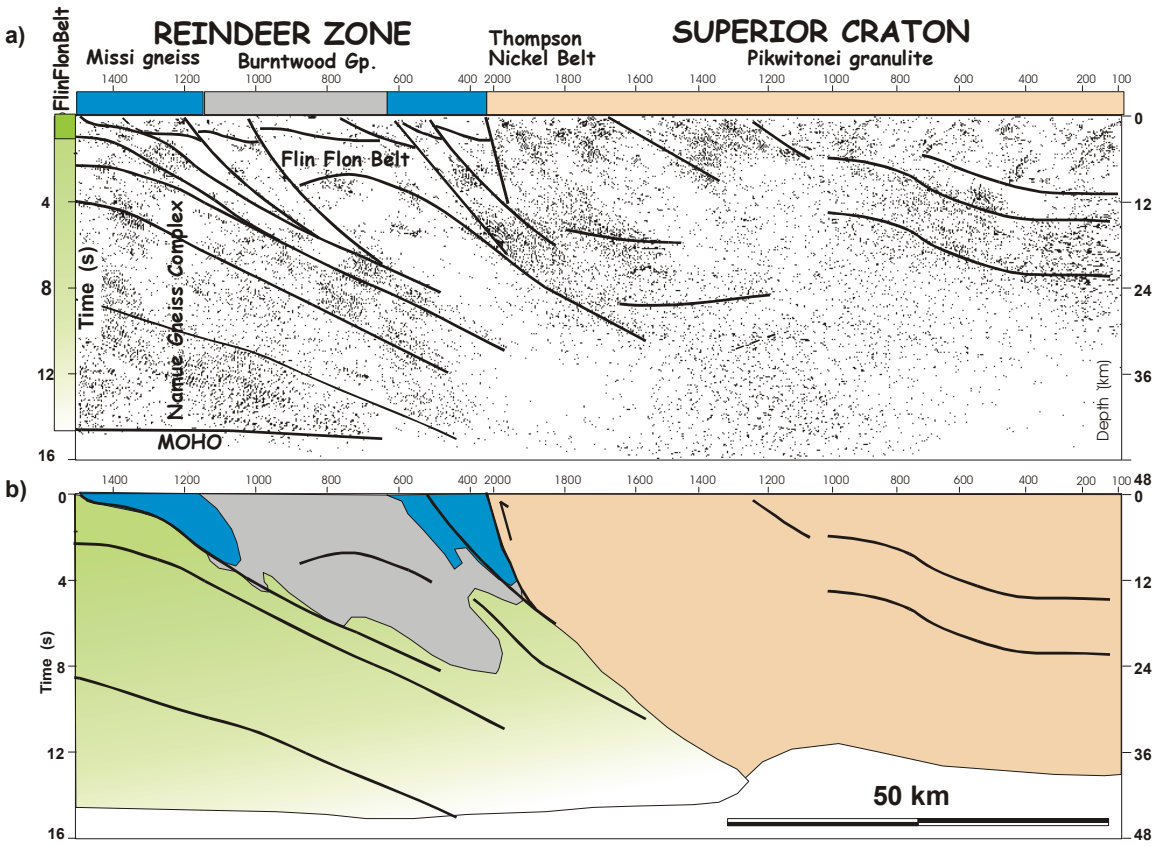

Figure 6.12 a) Seismic reflection profile (migrated and merged from two segments) crossing the Superior Boundary near Ponton. Line interpretation from White et al. (1999) showing reflectors dipping east under the TNB. b) Modified geological interpretation to conform with the thick-skinned ductile deformation found in the Kisseynew Domain. The depth of the Burntwood Group is unknown but taken to be bounded by strongly reflective crust.

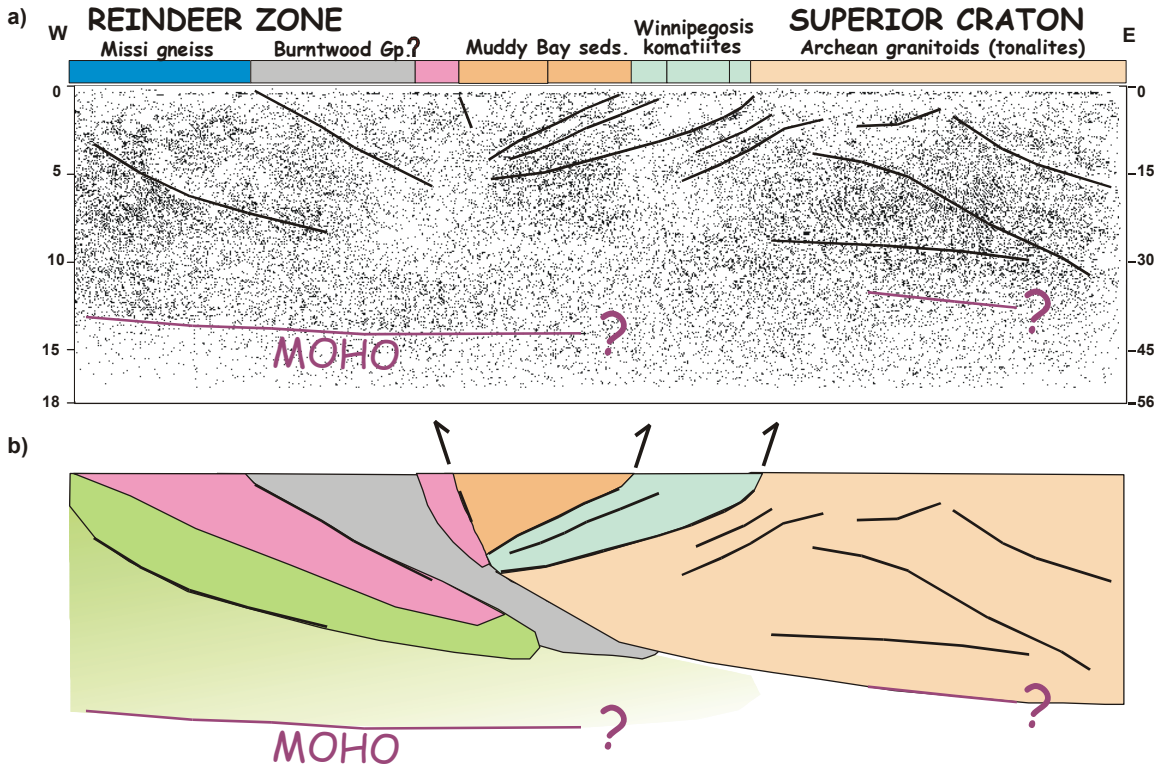

Figure 6.13 a) Seismic reflection profile (migrated) crossing the Superior Boundary near Easterville, on the Paleozoic rocks. Line interpretation from Lucas et al. (1996) showing reflectors dipping west over the Superior craton and east over THO, consistent with easterly thrusting followed by west-vergent structures. East-dipping reflectors in the Superior craton may be rift-related structures. b) Modified geological interpretation to conform with magnetic patterns that extend south from the Snow Lake area. The presence of the Burntwood Group is unknown. The Winnipegosis komatiite and tholeiite may occur in a westerly directed thrust belt.

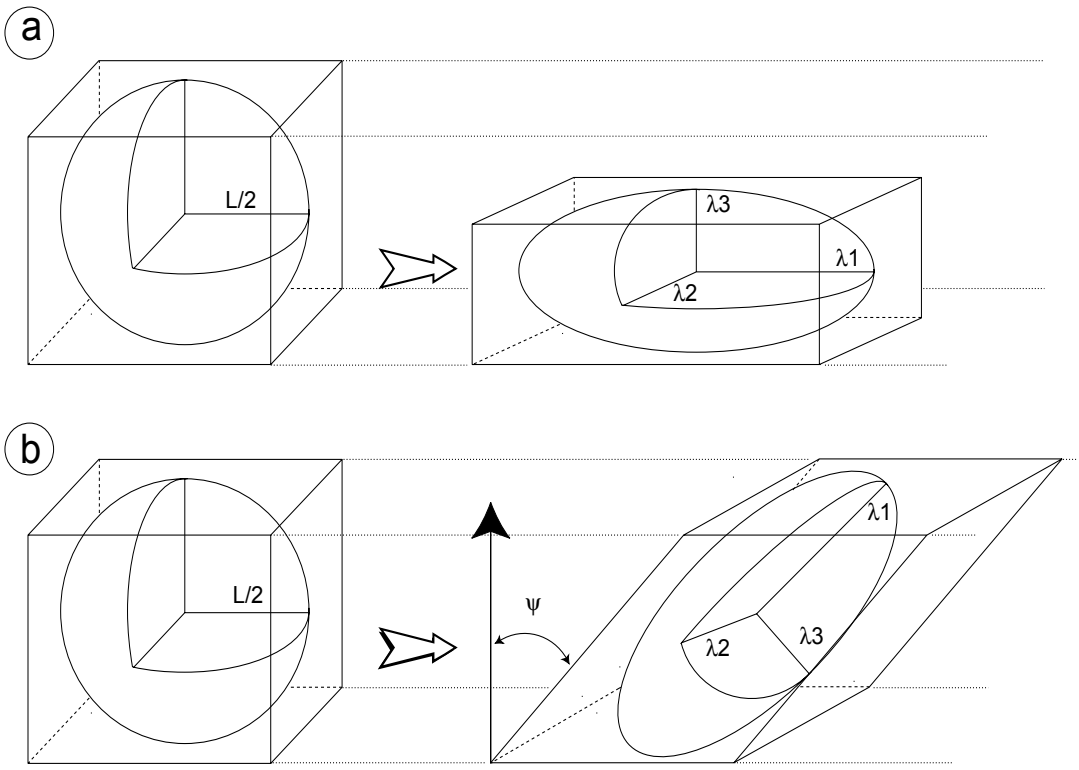

Figure 6.14 Transformation of a sphere during: a) pure shear (coaxial deformation); b) simple shear (non-coaxial deformation). ψ is the distortion angle.

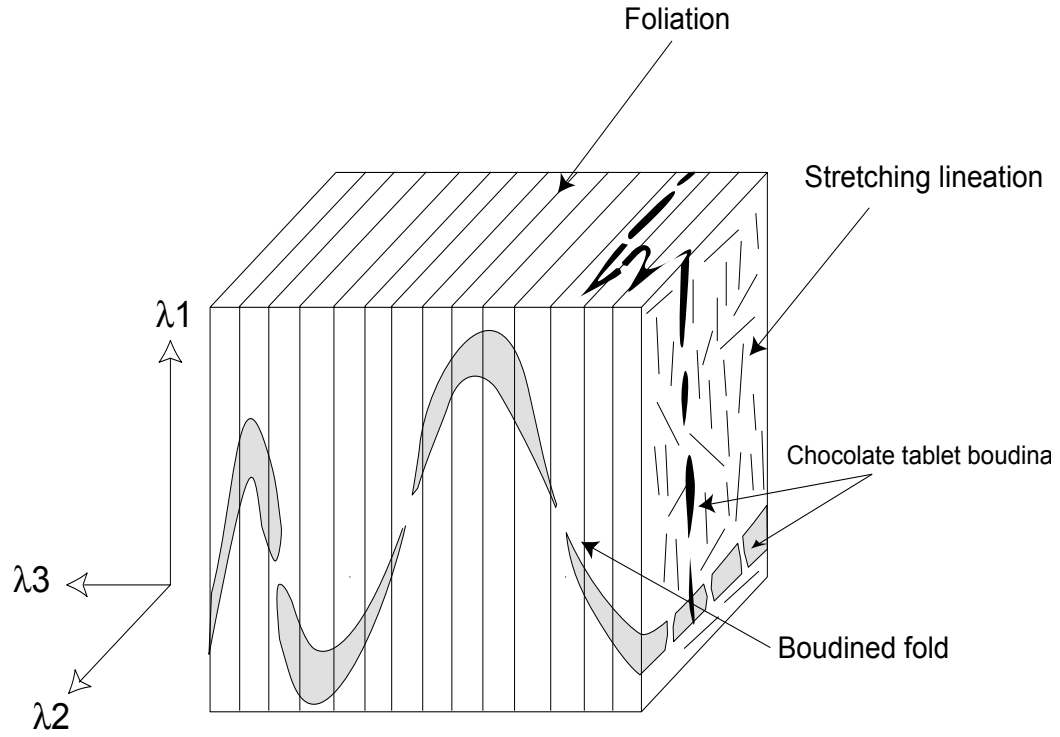

Figure 6.15 Orientation of structures relative to principal strain axis during flattening strain.

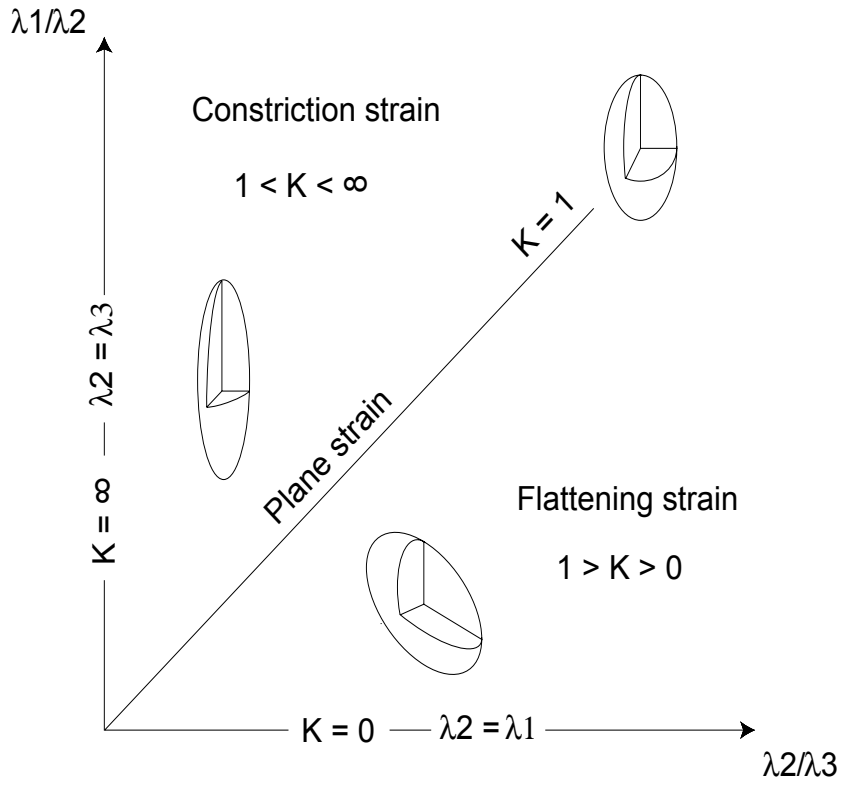

Figure 6.16 Different types of finite strain ellipsoids (after Flinn, 1962).

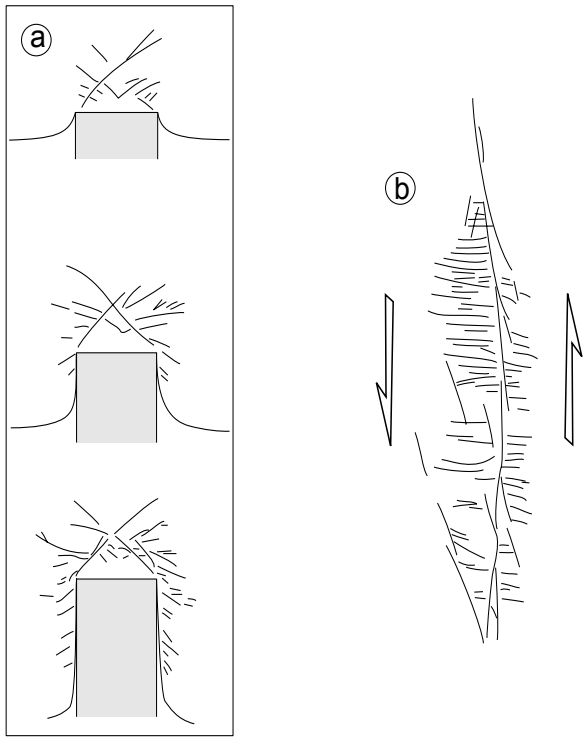

Figure 6.17 Experimentally produced fault

nets for: a) coaxial deformation (the net is symmetric in each stages of deformation: after Tapponnier et al., 1982); b) non-coaxial deformation (the net is asymmetric: after Tchalenko, 1970).

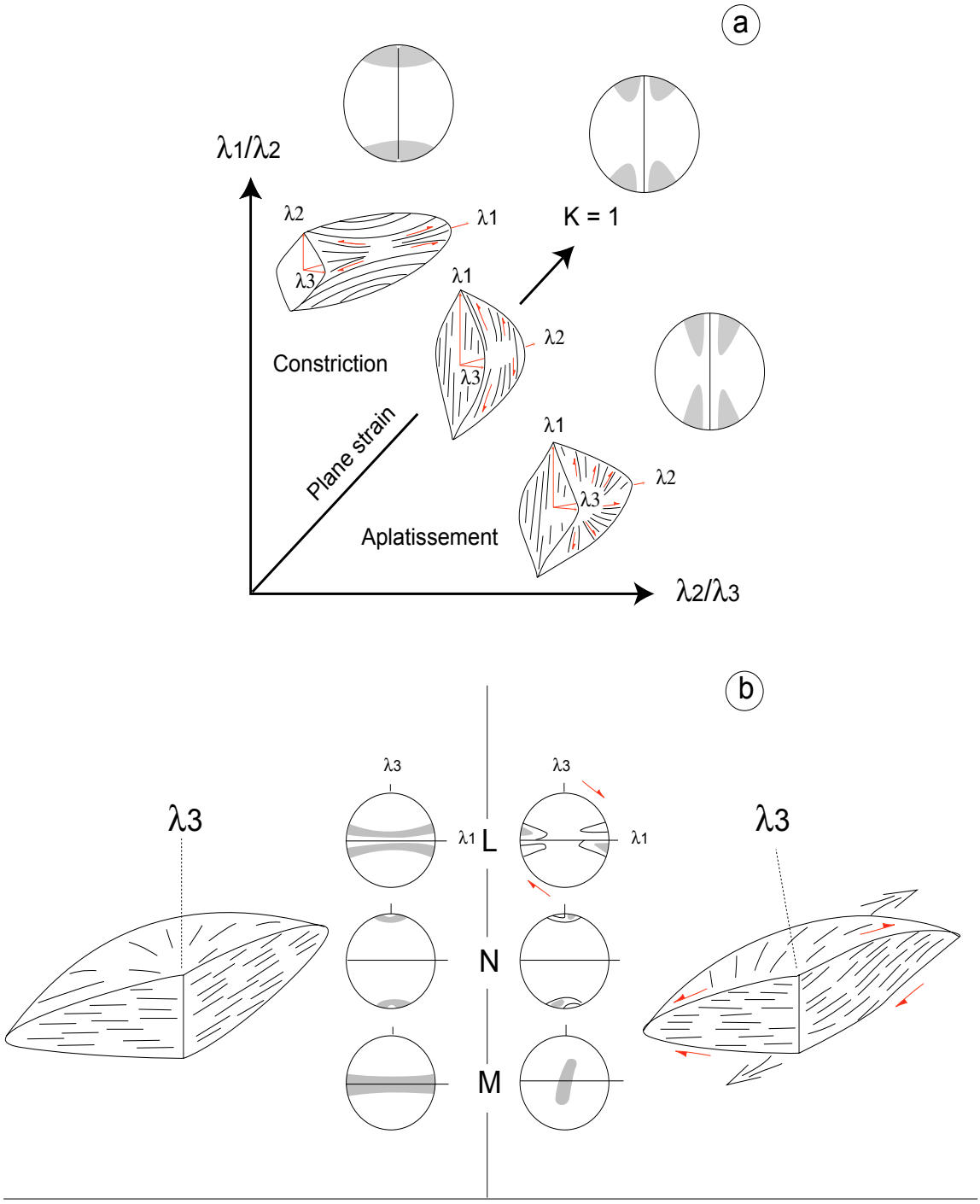

Figure 6.18 a) Flinn diagram showing expected geometry of shear zone arrays. Shearing surfaces and associated shear directions according to type of finite strain ellipsoid. Stereograms show ideal distributions of shear directions for bulk coaxial deformation (after Choukroune, 1995). b) Theoretical effect of bulk shearing deformation on the distribution of shear directions and shear senses on individual shear zones. Left-hand side, example of coaxial flattening; shear directions and shear senses are radially distributed on the lens-shaped shear surfaces. Right-hand side, example of non-coaxial flattening; shear directions are distributed on lens-shaped surfaces but are shifted toward bulk shearing direction. Stereograms show expected attitudes of shear directions (L), pole to shear zones (M) and normal to shear directions with individual shear zones (N). (After Gapais et al., 1987).

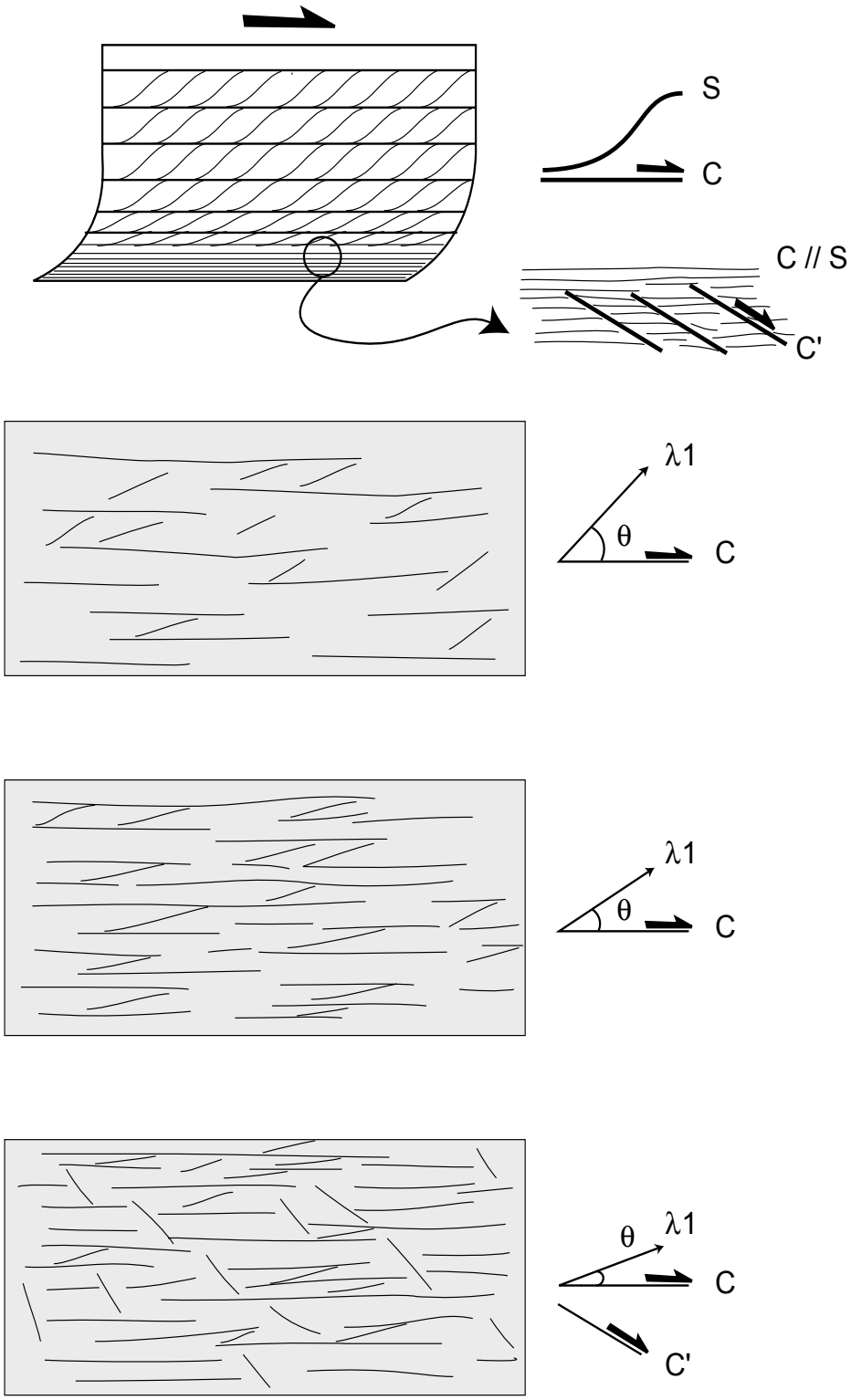

Figure 6.19 Example of progressive deformation: development of C/S/C' structures. The figures show the augmentation of C planes density, decrease of the angle between the C and S planes and appearance of the C' planes with increase of strain intensity (after Choukroune et al., 1987).

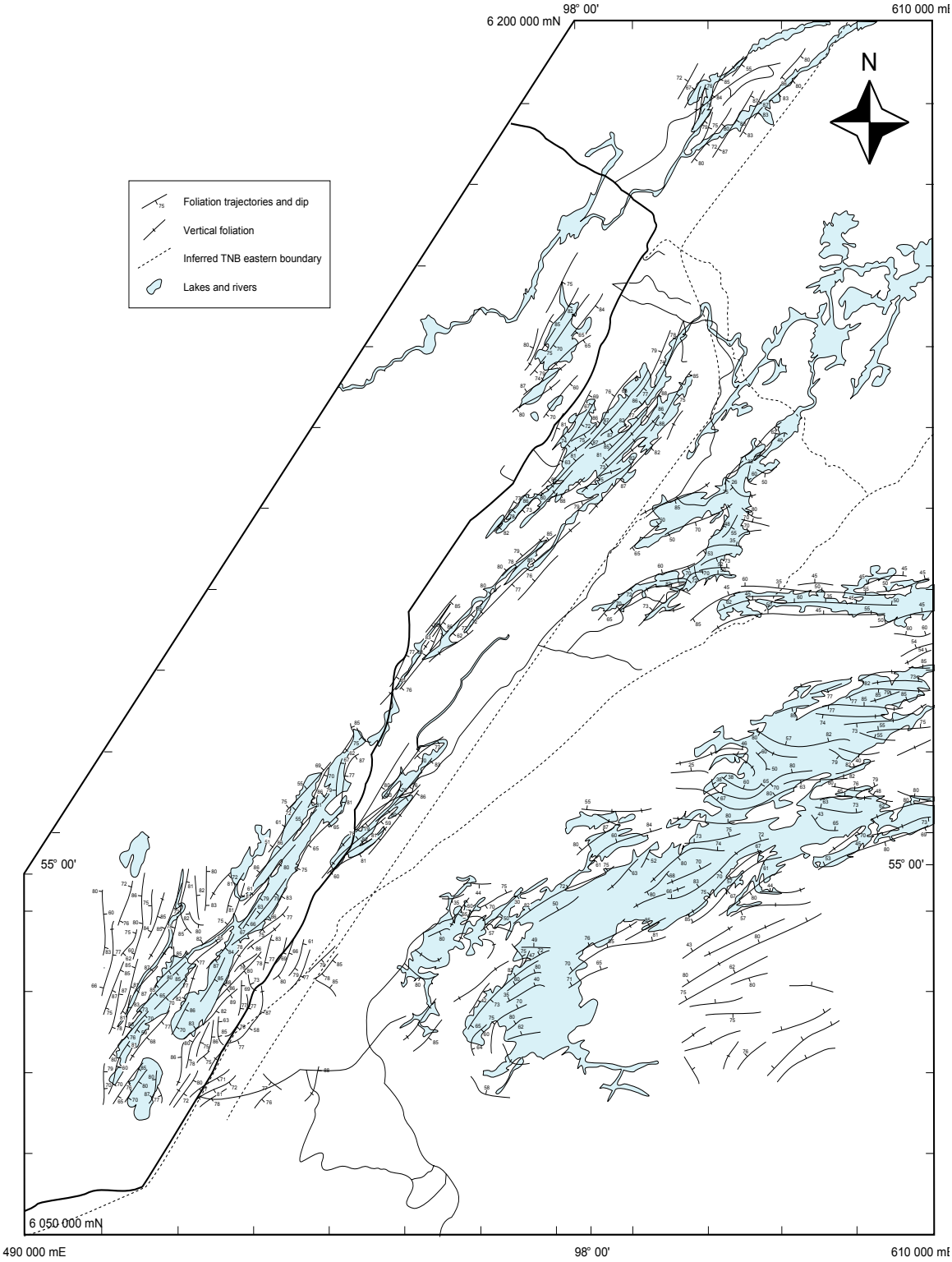

Figure 6.20 General foliation map of the TNB and adjacent eastern domain.

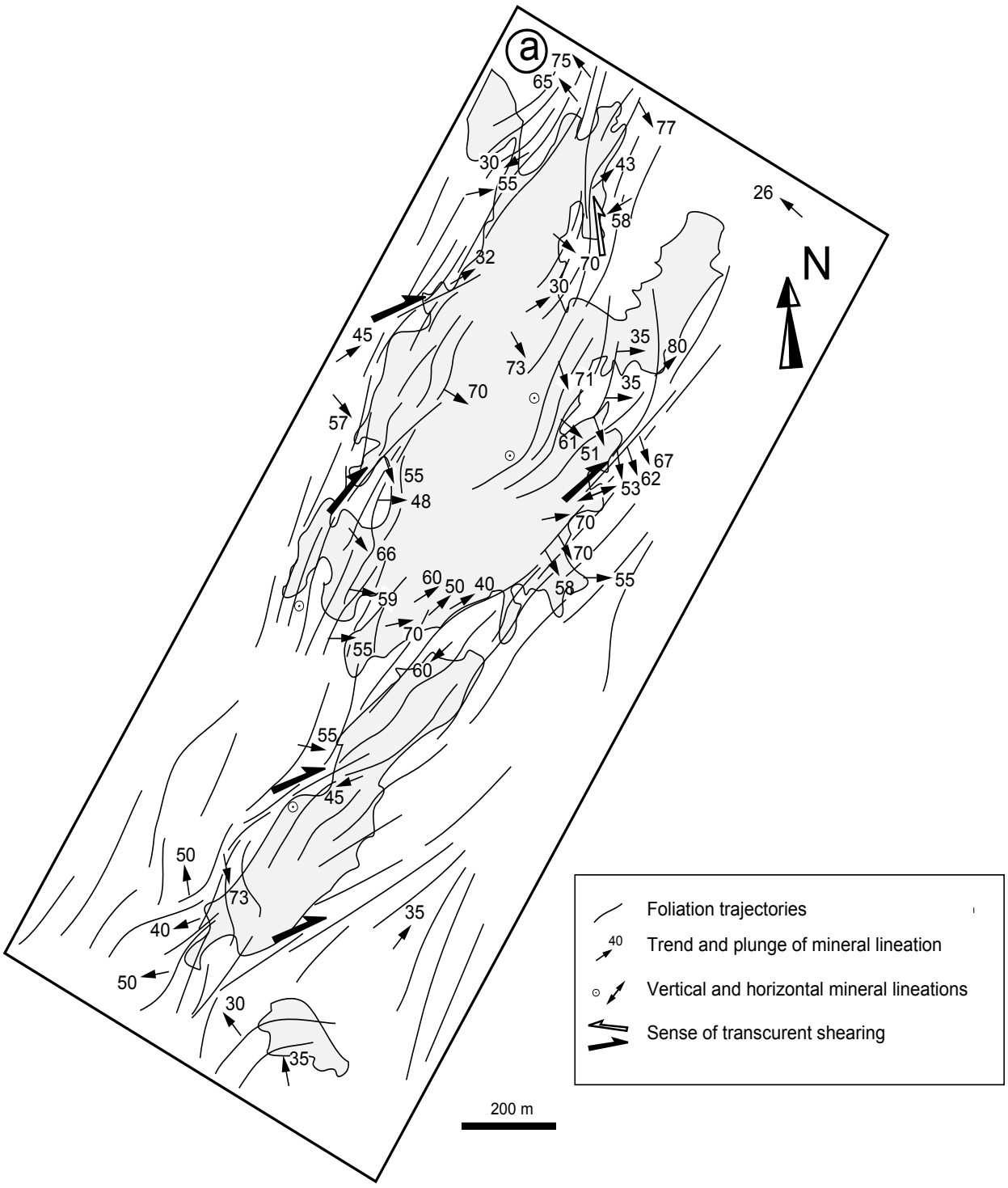

Figure 6.21 a) Ospwagan lake foliation trajectories and lineations map.

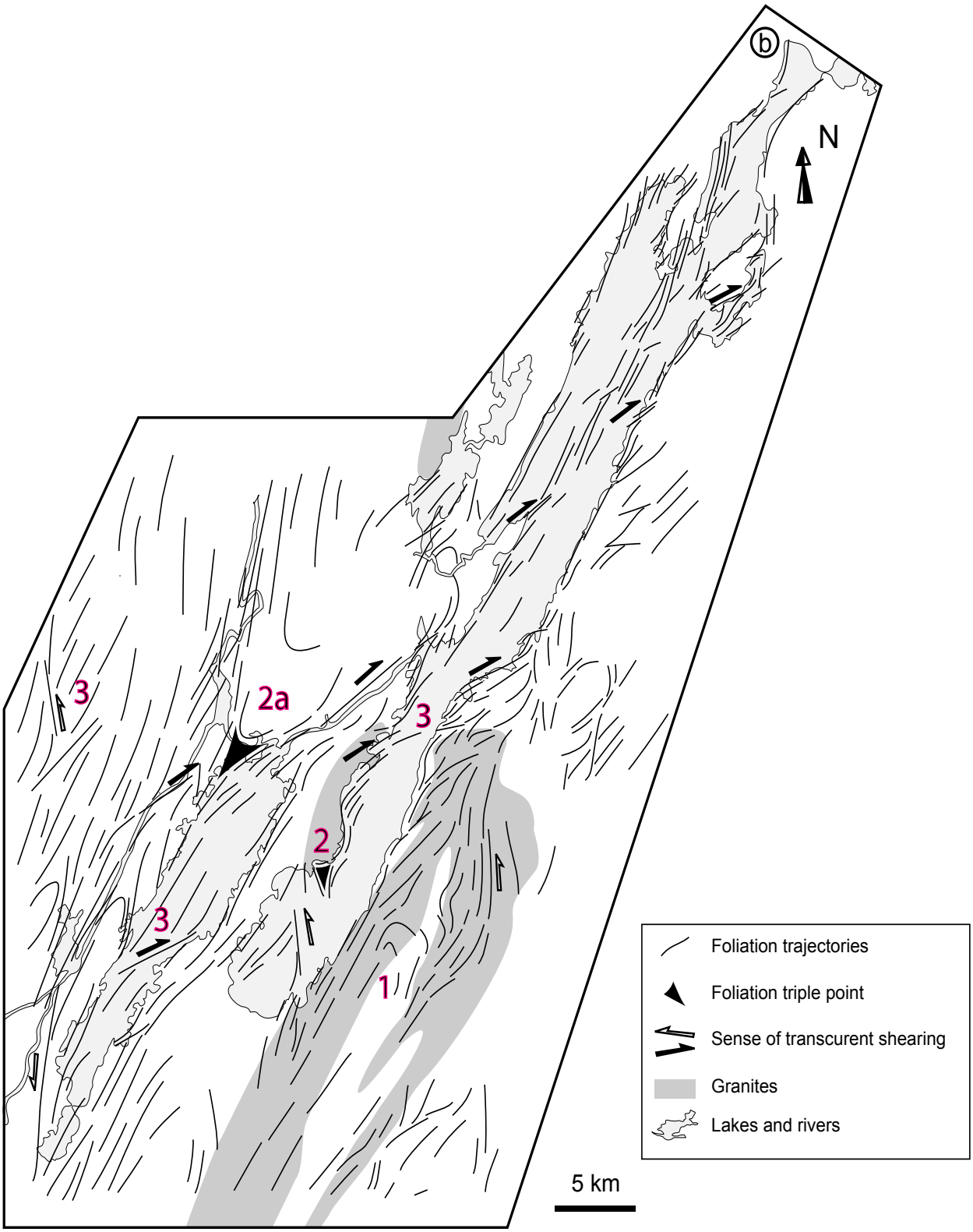

Figure 6.21 (cont.) b) Setting lake foliation trajectories map.

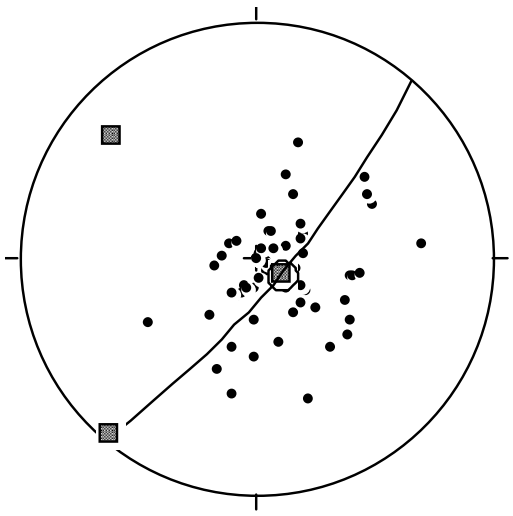

Stretching lineations

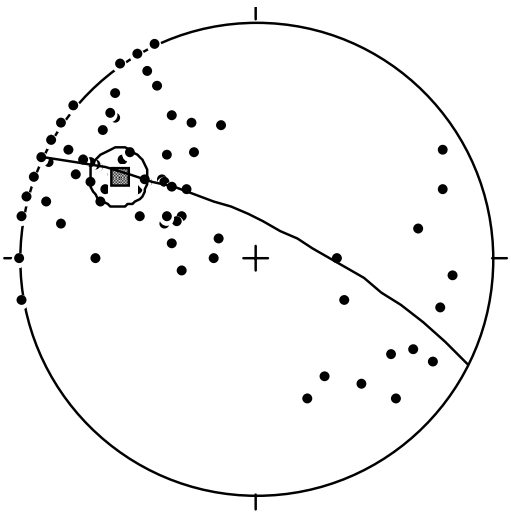

Foliation poles

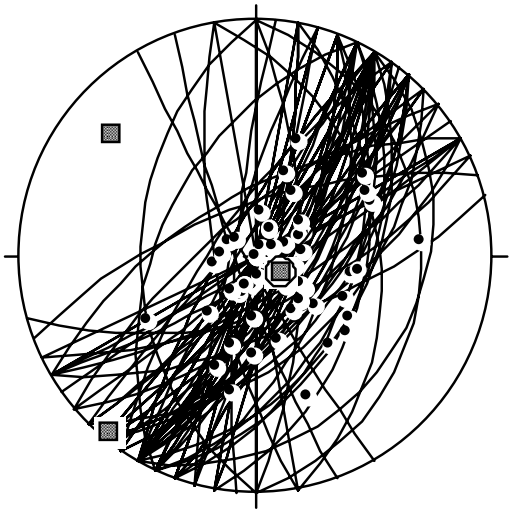

Mean lineation: 122°N/76.5°SE

Mean pole to foliation: 301°N/22°NW

Figure 6.22 Stereograms showing attitudes of regional stretching lineation (54 measurements) and foliation (100 measurements). Squares show corresponding principal directions.

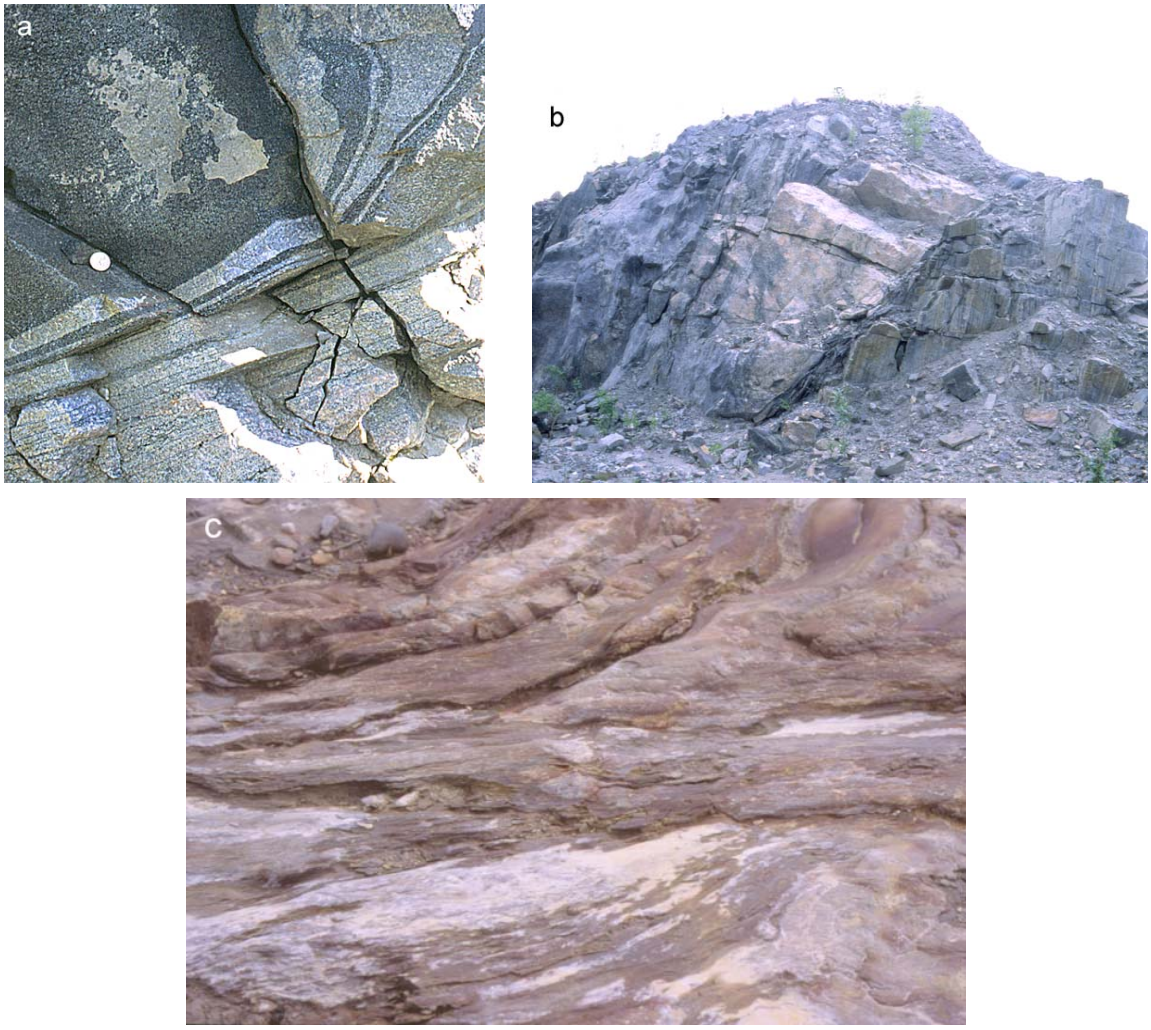

Figure 6.23 a) Top to the W thrust in amphibolite facies conditions, South Jonas road; b) Reverse top to the W fault, Thompson Pit T3; c) Dextral mineralized shear zone in greenschist facies conditions, Thompson T3.

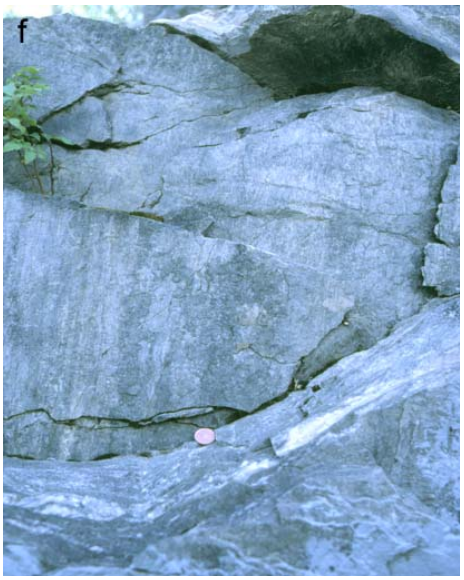

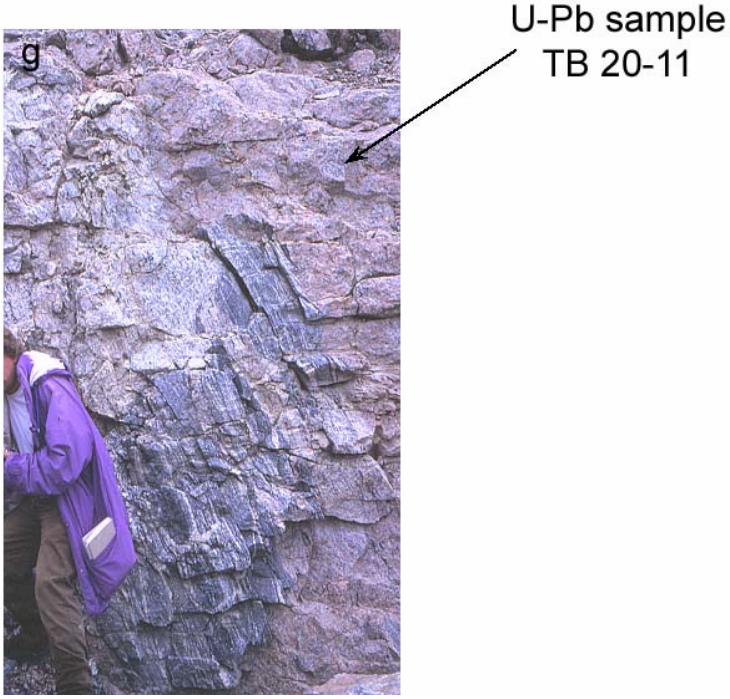

Figure 6.23 (cont.) d) Melt bearing dextral shear bands in the Archean gneisses, Thompson T3; e) Folded boudins in a pegmatitic vein intrusive within the Ospwagan sediments, Thompson T3; f) Vertical stretching on mylonitic schistosity; g) Post folial pegmatite associated with top to the W motion intrusive in the Archean gneisses. Dated sample TB 20-11 yields concordant ages ranging from 1820 ± 1 Ma and 1799 ± 1 Ma. South Jonas road.

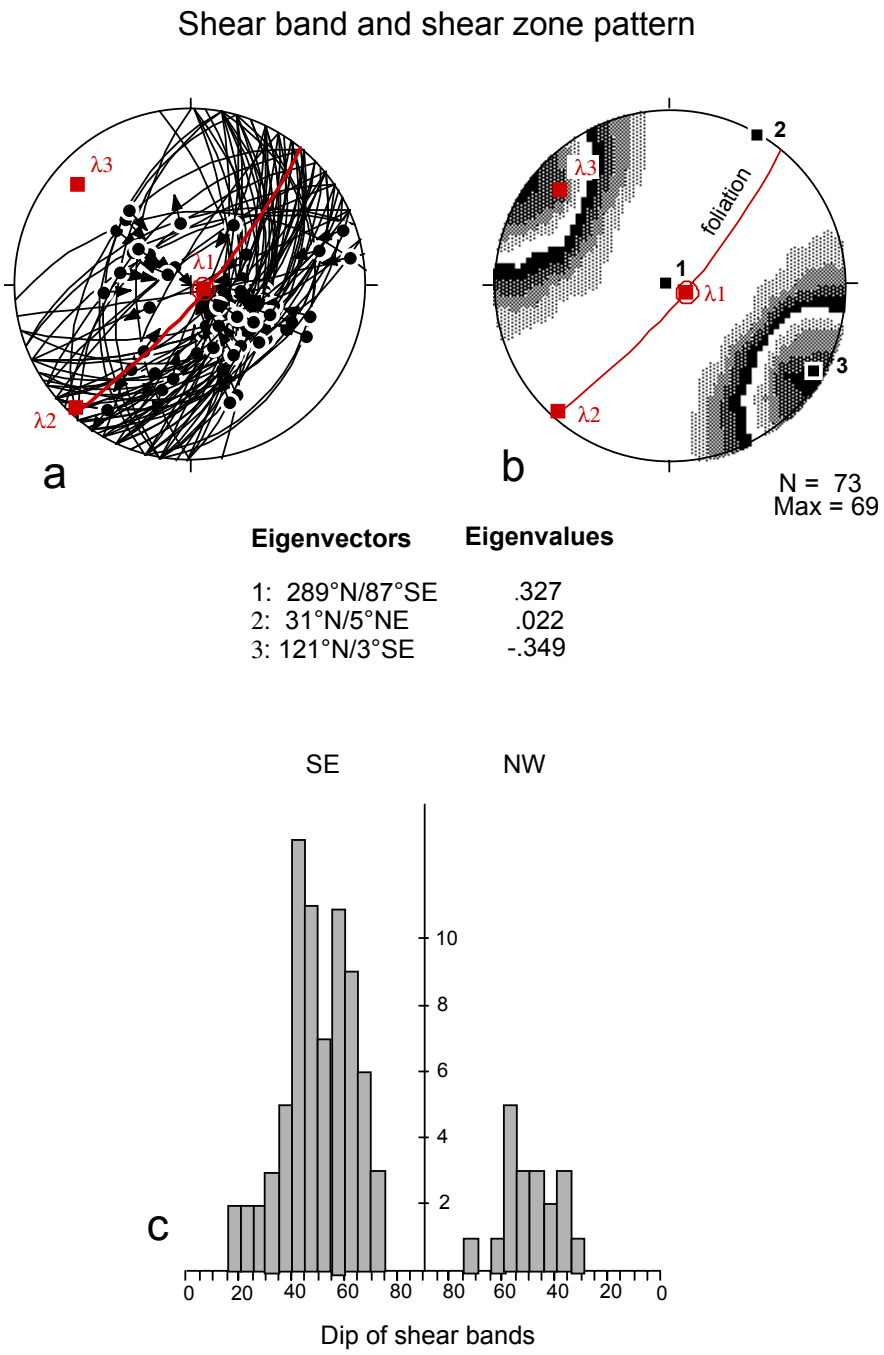

Figure 6.24 Distribution of shear zones and shear bands.

Upper figures: stereograms showing attitudes of individual bands and associated shear directions (arrow points indicate shear senses); mean stretching lineation and foliation are shown in red. Results show the application of the right-dihedra method (after Angelier and Mechler, 1979) to shear zone population. Contours underline preferred orientation of principal shortening direction on individual shear zones. 1, 2, and 3 are corresponding eigenvectors giving the best directions for bulk principal stretching (1), intermediate axis (2) and bulk principal shortening (3) for the studied population. N, total number of shear zones; max, number of kinematically compatible ones. The two eigenvalues are > 1, indicating stretching along both (1) and (2) principal directions.

Lower figure: frequency histogram of dips of measured shear zones, underlying that most dip SE.

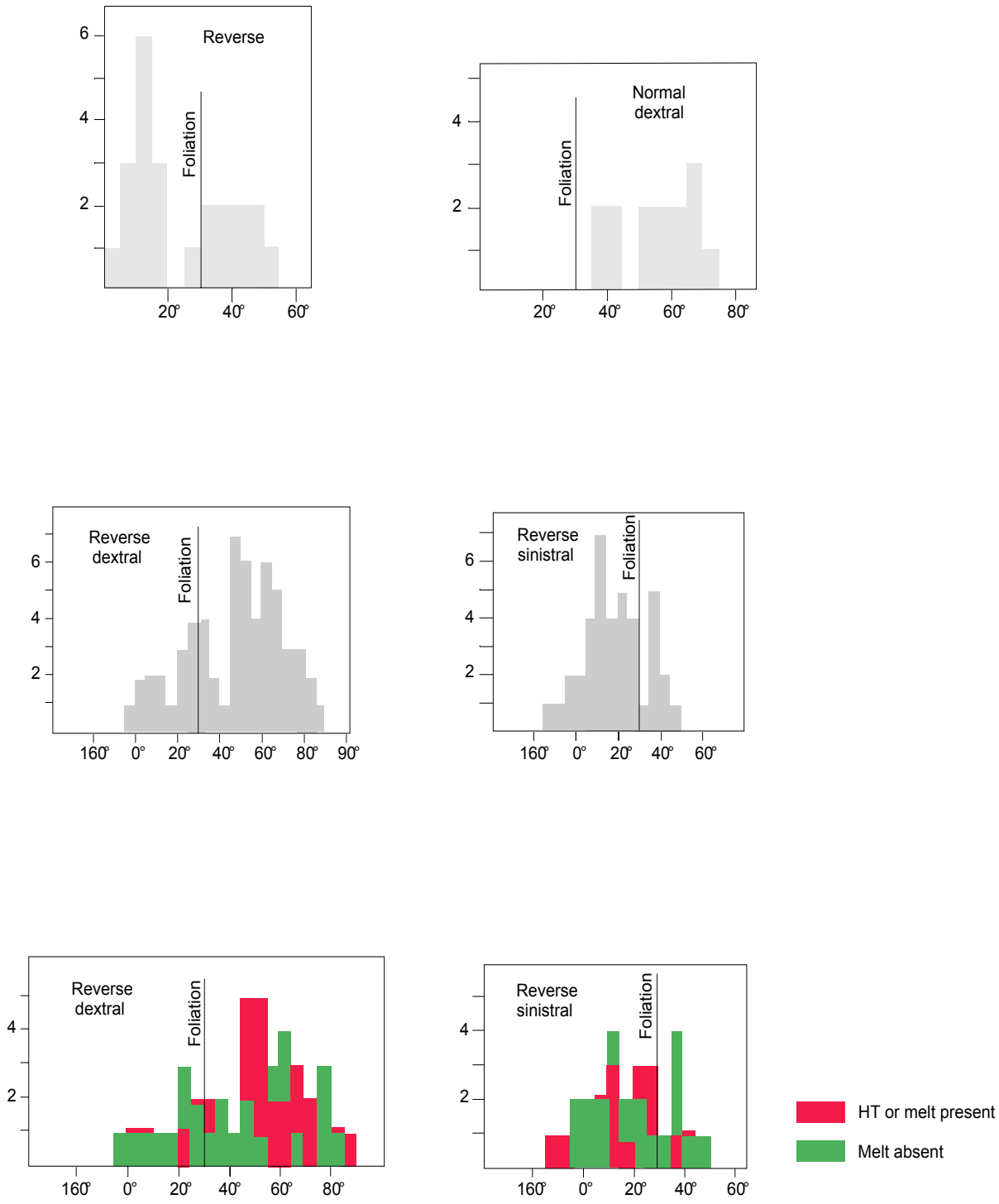

Figure 6.25 Frequency histograms showing distribution of measured shear zones according to their strikes and kinematics.

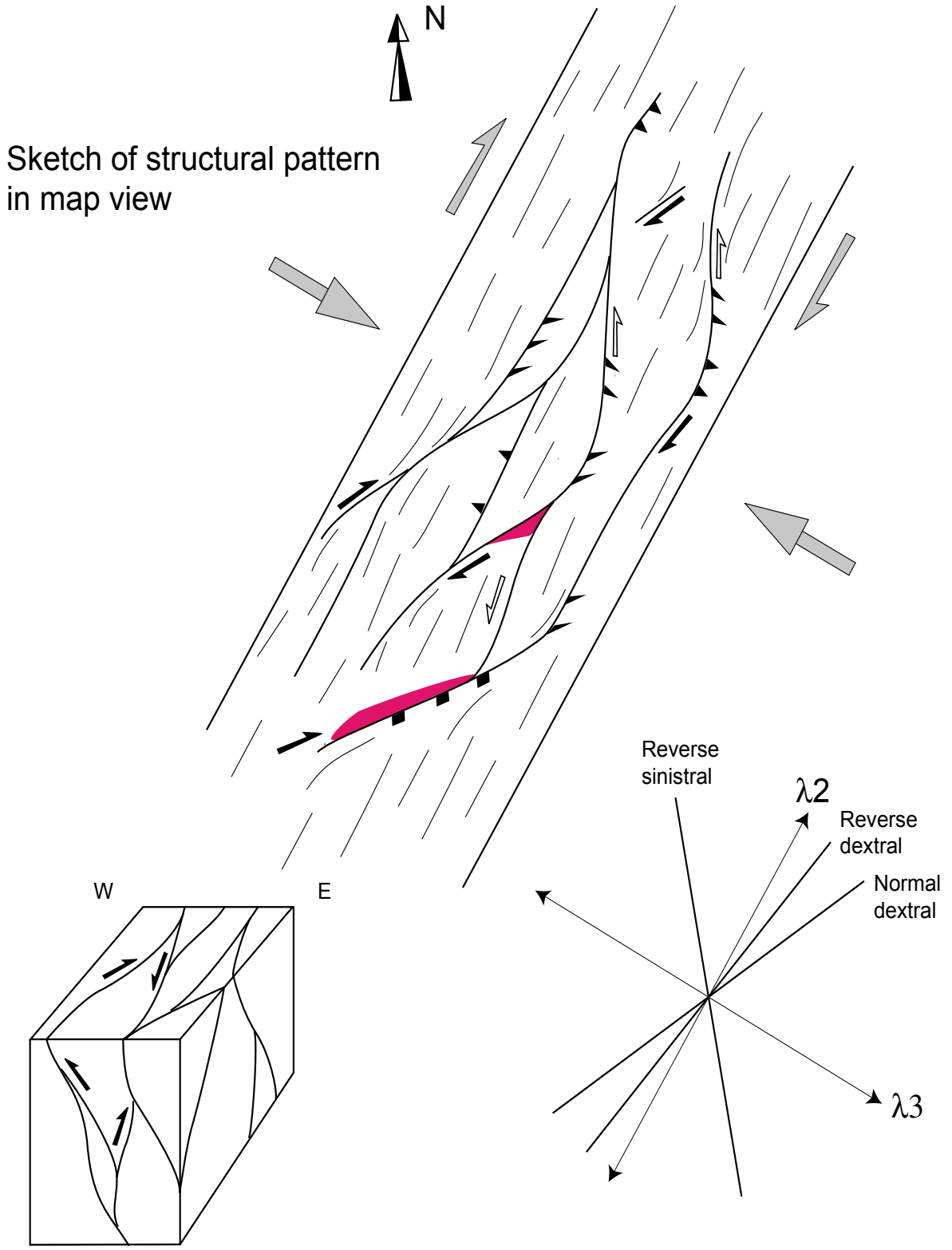

Figure 6.26 Cartoon illustrating the type of structural pattern observed in the TNB. Conjugate sets of reverse shear zones and shear bands show dominant top-to-NW motions combined with some components of dextral or sinistral strike-slip. The rose diagram shows dominant strikes of shear zones with respect to principal finite strain axes, according to their kinematics.